Part I

Radio-network planning

1 Framework automated tuning

The models and algorithms from Chapter **??** form the basis for the radio-coverage framework used throughout this thesis. Until here, the framework has been studied in the context of optimization-problem solving for radio networks.

In this chapter, the focus is shifted towards radio-network planning activities, and how the framework can aid a network-planning engineer in his or her everyday tasks. The objective is to facilitate refined network planning, the complexity of which is generally beyond the scope of any manual approach.

A central part of a radio-planning tool is its radio-propagation model. But the calculated signal-propagation predictions will be as good as the input data used for their estimation. Moreover, acquiring the necessary information to support the decision making in this context is a challenging task. In practical situations, an emitted signal propagates by interacting with the surrounding environments. Consequently, the ability of a propagation model to adapt to the environment where it is used improves the accuracy of the calculated signal-propagation predictions.

Within this context, this chapter presents two automated-tuning capabilities for PRATO. The first one involves the parameter tuning of the empirical radio-propagation model using a snapshot of field measurements. The second one involves the optimization of clutter losses over different regions of the country, therefore adapting the losses due to land usage to the local conditions of each region. The results of the experimental simulations, performed over three regions of the real LTE network deployed by Telekom Slovenije, d.d., show the suitability of the presented methods to improve the accuracy of the calculated radio-propagation predictions.

The content of this chapter extends the research work published by the author in ???. The rest of this chapter is organized as follows. Section **??** introduces principles of radio-propagation prediction, and the mathematical model used. The parameter-tuning problem and the analytical approach for tackling it are presented in Section **??**, including the simulations performed on the framework and their results. Section **??** concentrates on describing the optimization problem involving the regional adaptation of signal losses due to clutter, including the performed simulations the achieved results. Finally, Section **??** gives an overview of relevant publications, describing how they relate to our work, before drawing some conclusions.

1.1 Motivation

With the advent of long-term evolution (LTE) as the fourth generation (4G) in cellular technology, mobile operators are facing the challenges of deploying a new network. LTE follows the well established universal mobile telecommunication system/high-speed packet access (UMTS/HSPA) combo, targeting higher peak data rates, higher spectral efficiency and lower latency **?**.

The deployment of a new mobile network is always a challenge for mobile operators, who constantly struggle to find the optimal investment in order to provide a competitive network in terms of coverage and quality of service. Indeed, coverage planning remains a key problem that

all operators have to deal with. It has proven to be a fundamental issue since the deployment of the first GSM networks, more than 20 year ago.

One of the primary objectives of radio-coverage planning is to efficiently use the allocated frequency band for a geographic area to be satisfactorily reached with the radio stations of the network. To this end, radio-coverage prediction tools are of great importance as they allow network engineers to test different configurations before physically implementing the changes. However, to accurately predict the radio coverage of a mobile network is a very complex task, mainly due to the wide range of various combinations of hardware and configuration parameters which have to be analyzed in the context of different environments. The complexity of the problem means that radio-coverage prediction is generally a computationally-intensive and time-consuming task, hence the importance of fast and accurate prediction tools.

Although different mathematical models have been proposed for radio-propagation modeling, none of them excels in a network-wide scenario **?**. Empirical propagation models usually give good results with a limited computational effort. However, for improved accuracy, the model parameters have to be adapted to better fit a specific network or region within it, mainly because of inaccuracies in input data and environmental changes in the network region, e.g. foliage of trees or snow. Consequently, a combination of different parameters is generally needed in order to reliably calculate radio-propagation predictions for particular environments. Moreover, since the number of deployed cells (transmitters) keeps growing with the adoption of modern standards **?**, there is a clear need for a radio propagation tool that is able to cope with larger work loads in a feasible amount of time.

To address the afore-mentioned issues, we adapt the parameters of an empirical propagation model to a set of field measurements. The parameter tuning is analytically calculated per cell, in order to increase the accuracy of the calculated predictions. Moreover, we fine tune the signal losses due to land usage (clutter) in a regional basis, using an optimization approach. As a working framework to tackle the presented problems, we use a parallel radio-prediction tool **?**, thus showing the suitability of the presented framework for real-world planning and optimization of LTE radio networks. Particularly, we show the tool capabilities to handle several parallel radio-prediction runs using a metaheuristic algorithm and distributed objective-function evaluation, while resolving the clutter optimization problem.

1.2 Related work

There are few examples of radio-network simulators in the literature **??????**. Most of these tools were developed for academic research, thus not targeting industrial-sized environments.

A Matlab-based LTE simulator was proposed in **?**. It implements a standard LTE downlink physical layer, including Adaptive Modulation and Coding (AMC), multiple users, MIMO transmission and scheduler. Despite being open source and freely available, the fact of being implemented in Matlab makes it restrictive in terms of tackling big problem instances of real networks.

A promising tool from the performance point of view was presented in **?**, where the authors implemented a full-stack LTE system in C++. Although the tool has no graphical capabilities for displaying the simulation progress or outcome, they might be included, since the source code is available. In our opinion, the main drawback of this tool is the lack of documentation, which makes it very difficult to continue extending this work without the direct help of some of the original authors.

As an extension to the well-known NS-2 network simulator, Filiposka and Trajanov **?** introduced a module for radio-propagation predictions, which takes the terrain profile into account.

In this case, the authors focus on the relief, leaving out signal loss due to land-usage, which is an important factor when targeting realistic radio-propagation scenarios.

Following an optimization-oriented approach, the authors of **?** study the effects on location accuracy while performing semi-automated optimization of the parameters of a radio-propagation model. While their optimization component improves the accuracy of the radio predictions, it does so requiring human intervention, hence the term semi-automated optimization. In terms of the effects of location accuracy, they conclude that locations with a median accuracy of around 60 m may be used for parameter tuning. Also, they notice that although the model accuracy improved after the parameter tuning, it gives inadequate results when used for predicting radio propagation over distant areas.

1.3 Parameter tuning of the radio-propagation model

The effectiveness of the decision-making process during radio-network planning is tightly coupled with the precision achieved by the propagation model used. In order to obtain a radio-propagation model that most accurately reflects the propagation characteristics of the area covered by each radio cell in the network, the parameters of the mathematical model should be adapted to the environment into which it is to be used. The current state-of-the-art method for such parameter tuning depends on existing field-measurement data **??**, which are collected in advance for the area covered by the target network cells. Starting from an a-priori best-known set of parameters, empirically calculated by the radio engineers at Telekom Slovenije, d.d., this approach adapts the model parameters so that the deviation of the radio-propagation prediction to a given set of field measurements is minimized.

To calculate the radio-propagation predictions, the empirical radio-propagation model, previously introduced in Chapter **??**, Section **??**, is used. Recall that the model contains a vector of adaptable parameters, β. For this reason, this mathematical model is especially appropriate for tuning, since it can be adapted to a given scenario and its local conditions by adjusting the values of the vector $\beta = (a_0, a_1, a_2, a_3)$, the elements of which represent

a_0 the reference loss or offset;

a_1 the loss slope due to distance of the receiver from the transmitter;

a_2 the loss slope due to height of the transmitter antenna;

a_3 the loss slope due to the combined effect of the distance and height of the antenna.

The parameter tuning is performed per cell to improve local fitting of the radio predictions, being its resulting solution a vector β_c for the target cell $c \in C$.

Also, recall that the model includes an extra term in order to adequately predict signal-loss effects due to foliage, buildings and other fabricated structures. These loss factors are based on the land usage, i.e., clutter data. Here, twelve different clutter categories are recognized. Table 1.1 lists these categories, including their label numbers and descriptions.

1.3.1 Field measurements

In mobile networks, a moving mobile device (or user equipment, UE) constantly performs cell selection/reselection and handover (see Chapter ???, Section ???) in order to keep the best possible connection to the network. Within this context, the best connection is selected by measuring the signal strength or quality of the neighboring cells. In LTE networks, the UE

Table 1.1: Clutter-category label numbers and descriptions for the signal-loss due to clutter of the radio-propagation model.

Clutter category	Description
0	Urban area without buildings, mostly roads
1	Suburban area
2	Urban area
3	Dense urban area
4	Agricultural area
5	Forestall area
6	Swamp area
7	Dry open land area with special vegetation
8	Dry open land area without special vegetation
9	Water area
10	Industrial area
11	Park area

measures two parameters from the reference signal of the network, namely the Reference Signal Received Power (RSRP) and the Reference Signal Received Quality (RSRQ).

For a certain frequency bandwidth, RSRP measures the average received power over the resource elements that carry cell-specific reference signals. RSRP is applicable in both idle mode (e.g., waiting for a call) and connected mode (e.g., during a call). During the procedure of cell selection/reselection in idle mode, RSRP is used. On the other hand, RSRQ is only applicable when the UE is in connected mode.

The radio-propagation prediction involves calculating the network coverage over a certain region, and thus to the UEs within it. Hence, in the first place, the focus is on accurately predicting the best connection the UE would select in idle mode and the RSRP measurements it uses.

Here, the field measurements representing the RSRP at a given location were collected using a small truck equipped with a spectrum analyzer. The spectrum analyzer is connected to an external omni antenna mounted on the roof of the truck, at roughly 2 m above the ground, taking measurements at a rate of 2 Hz. To accurately establish their location points, a GPS unit was used. These GPS-informed locations have been tested to be compliant with the 60 m limit mentioned in **?**. The measurements cover most of the streets within the target area, with over 300,000 individual points, collected for more than 140 network cells.

To minimize the error impact in measured RSRP, all field measurements are processed so that a single value, the median, is calculated for each of the measured locations. This processing step improves measured-data quality in terms of possible deviations due to external factors, e.g., driving speed. The resulting RSRP is then used to estimate the path-loss prediction at the corresponding location, the resolution of which matches that of the DEM and clutter data.

1.3.2 Linear least squares

The approach for tuning of the radio-prediction model is to correlate the field measurements with the predicted received-signal values, i.e., RSRP. The new parameter set originates from the

Table 1.2: Several properties of Net_8, Net_9 and Net_{10}, the test networks used for the experimental simulation of the framework automated tuning.

	Number of cells	Area (km^2)	Field-measurement proportion (%)
Net_8	12	103.74	5.41
Net_9	130	1298.02	12.02
Net_{10}	6	386.38	2.30

minimization of an error criterion. Similar to **???**, the minimization criterion is the squared-sum difference between the predicted and the observed RSRP levels, i.e.,

$$E(\beta_c) = \sum_{i=1}^{m_c} (p_c - pl_c(i, \beta_c) - fm_i)^2, \tag{1.1}$$

where $E(\beta_c)$ is the observed error for cell c given the parameters β_c, p_c is the transmit power of cell c, and $pl_c(i, \beta_c)$ is the path loss of cell c at the same geographical point of fm_i, i.e., the i-th field measurement out of a set of measurements for cell c, with cardinality m_c.

A necessary condition for the linear least-squares method to find the global minimum is the linear relationship between the predicted path loss, $pl_c(i, \beta)$, and the vector β_c **?**. This condition can be verified by calculating the first derivative of $E(\beta_c)$ in terms of the of components of vector $\beta_c =< a_{0c}, a_{1c}, a_{2c}, a_{3c} >$, i.e., $\frac{\partial E(\beta_c)}{\partial a_{0c}} = 0$, $\frac{\partial E(\beta_c)}{\partial a_{1c}} = 0$, $\frac{\partial E(\beta_c)}{\partial a_{2c}} = 0$, and $\frac{\partial E(\beta_c)}{\partial a_{3c}} = 0$.

1.3.3 Simulations

The simulations carried out for this part of our work consist of building the matrices of observed-error values, $E(\beta_c)$, for each cell c in the target network. The linear systems of equations are then individually solved by applying the linear least squares method presented in the previous section, which involves the evaluation of one radio-coverage prediction per cell. Each solved system holds a unique solution for a cell c, $c \in C$, denoted by the vector β_c.

1.3.3.1 Test networks

The test networks, Net_8, Net_9, and Net_{10}, are subsets of a real LTE network deployed in Slovenia by Telekom Slovenije, d.d. The path-loss predictions are calculated using PRATO, with a DEM and clutter map of 25 m^2 resolution, and a receiver height of 2 m above ground level. A transmission radius of 16 km defines the coverage prediction area around each network transmitter, thus limiting the path-loss prediction to a distance where it is feasible for a UE to connect to a cell, with a RSRP greater or equal to -124 dBm **?**. At the same time, the selected transmission radius provides enough overlap among neighboring cells to calculate the network coverage over the whole region. Table 1.2 provides more information about the test networks used, showing the number of network cells, the area surface, and the covering proportion of the collected field measurements in terms of the total area of each test network.

Net_8 represents a network deployed over a dominant agricultural area with almost flat terrain, some forests and waters streams. Net_9 is deployed over a densely populated urban area, containing high buildings, parks and avenues. The last one, Net_{10}, represents a network deployed over hilly terrain, including some smaller villages and vast forests. It is important to note that the number of deployed cells is directly related to the population density within the region of each test network. This relationship can be derived from the information listed in Table 1.2, where the number of cells is shown along the area of every test network. For a clearer characterization

Table 1.3: Clutter-category proportions, expressed in percent, in terms of the surface area of each of the test networks. The category legend is given in Table 1.1.

	Cat. 0	Cat. 1	Cat. 2	Cat. 3	Cat. 4	Cat. 5	Cat. 6	Cat. 7	Cat. 8	Cat. 9	Cat. 10	Cat. 11	Total
Net_8	0.53	4.53	1.68	0.45	71.89	17.94	0.07	0.00	0.03	2.21	0.67	0.00	100.00
Net_9	0.91	5.53	9.48	3.84	29.73	48.57	0.14	0.03	0.03	0.76	0.86	0.12	100.00
Net_{10}	0.15	3.99	1.14	0.11	26.50	67.13	0.26	0.00	0.00	0.36	0.36	0.00	100.00

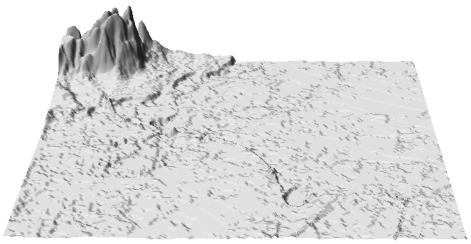

Figure 1.1: Terrain profile of test network Net_8, dominated by a flat agricultural area.

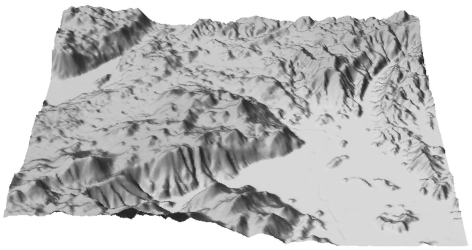

Figure 1.2: Terrain profile of test network Net_{10}, dominated by forested hills.

of the test networks in terms of terrain types and their extent, the proportion of each clutter category with respect to the total area of every test network is shown in Table 1.3.

The terrain profiles are most relevant for Net_8 and Net_{10}, since none of them contains densely populated urban areas. Note that the terrain shown in Figure 1.1 is mostly flat, since the agricultural area prevails in Net_8. In contrast, the terrain for Net_{10} is dominated by hills, which are mostly covered by dense forests, including some small villages in the valleys (see Figure 1.2).

In the following, the default parameters of the radio-propagation model correspond to the values provided by the engineers of the Radio Network department at Telekom Slovenije, d.d.

1.3.3.2 Experimental environment

The simulations were carried out on several computing nodes of the previously presented DEGIMA cluster **?** at the NACC of the Nagasaki University in Japan (see Chapter **??**, Section **??**). Groups of 3, 4, and 34 nodes were used for executing the simulations of the different problem instances, i.e., Net_8, Net_9 and Net_{10}, respectively.

1.3.4 Results

The results of applying the linear least squares method to fit the parameters of the radio-propagation model to a set of field measurements are presented in this section. Bar charts were prepared to show the cumulative distribution of the absolute error between the radio-propagation prediction and the field measurements (see Figures 1.3, 1.4, and 1.5). Each bar represents an open interval, expressed in dB, denoting the proportion of points that deviate from the prediction in the given number of dB. For example, in Figure 1.3 (a), it can be observed that the proportion of predicted points differing from the field measurements in 35 dB or more is around 16%, whereas the proportion differing in less than 5 dB is 10%. These values correspond to the test network Net_8 before applying the model-parameter fitting. For comparison, in Figure 1.3 (b), the absolute-error distribution for the same test network is given, but with the model parameters

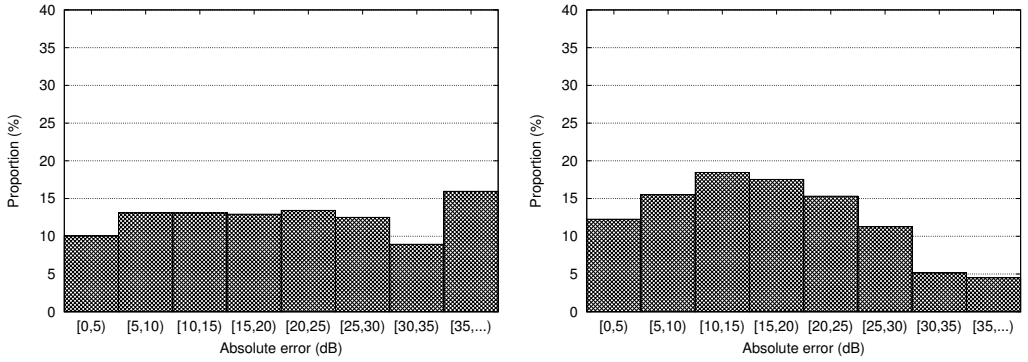

Figure 1.3: Error distribution of the radio prediction for network Net_8: (a) with default parameter values, and (b) with fitted parameter values.

fitted to the available field measurements. Notice how the proportions describing the biggest deviation have dropped to under 5% (35 dB and more) and to less than 6% (30 dB to 35 dB), respectively. Moreover, it is clear how all proportions improved, raising the bars towards the left-hand side of the chart and lowering them on the right-hand side.

The error distributions of the radio-propagation prediction for test network Net_9 using the default parameters and the fitted ones are given in Figures 1.4 (a) and 1.4 (b), respectively. In this case, the improvement is even more significant than for the previous test network, clearly showing that the tuned propagation model represents the local radio propagation conditions more accurately.

For the last test network, Net_{10}, the error distributions are depicted in Figure 1.5 (a) using the default parameters, and Figure 1.5 (b) for the tuned ones. Similar to the first test network, Net_8, it can be clearly seen how the proportions of highest error deviations have been lowered with respect to those with lower deviation values.

The overall results confirm that fitting the parameters of the radio-propagation model to the field measurements of each network cell significantly improves the quality of the calculated radio-propagation predictions. Indeed, since the default parameters were provided by the radio engineers after following a traditional configuration approach for the whole network, we may conclude that our automated fitting method is not only simpler, but also superior in terms of solution quality.

However, it is worth pointing out the particular reasons behind the considerable better results for Net_9, when compared to those of Net_8 and Net_{10}. Clearly, the relative quantity of available field measurements directly affects the quality of the calculated results, making the least squares approximation rougher and thus less precise for the networks where the field-measurement proportion is lower. See Table 1.2 in Section 1.3.3.1 for a reference of the field-measurement proportions with respect to the area surface of each test network. Similar findings were confirmed by other authors, who worked on the adjustment of radio-propagation models to different environments **?**. For the sake of completeness, it is worth pointing out that some researchers have already started working on different ways on how to improve this aspect **??**.

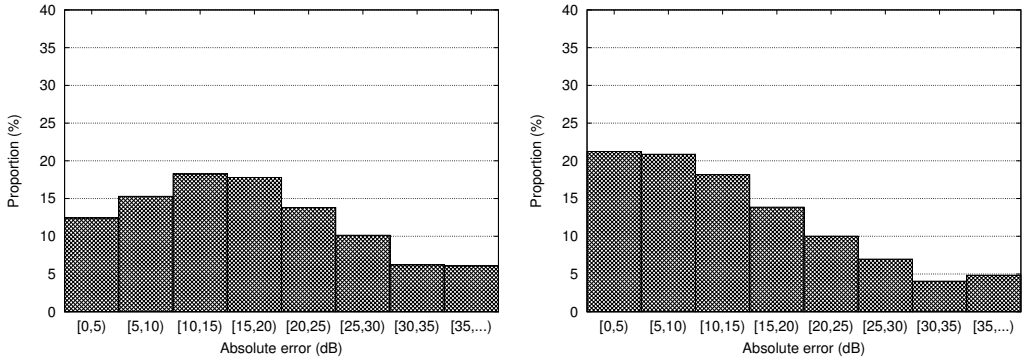

Figure 1.4: Error distribution of the radio prediction for network Net_9: (a) with default parameter values, and (b) with fitted parameter values.

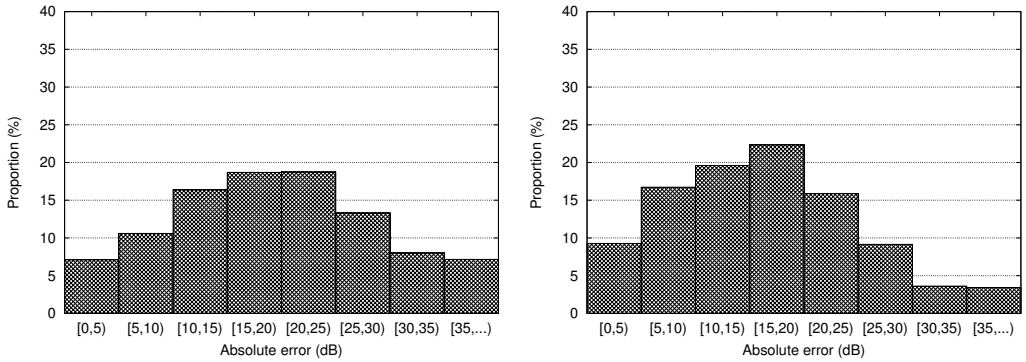

Figure 1.5: Error distribution of the radio prediction for network Net_{10}: (a) with default parameter values, and (b) with fitted parameter values.

1.4 Clutter optimization

In order to further improve the accuracy of the radio-prediction calculation over a given regional environment, the signal losses due to clutter have to be optimized. As it was mentioned before, there are several reasons for the predicted signal-loss values to be inaccurate. Seasonal changes are also among them, like tree foliage or snow, demolition or construction of buildings and parks, different kinds of forests or agricultural areas, etc. These changes are only noticeable through regular updates of accurate land-usage data. However, in the short term, updates are only available in the form of feedback by means of field-measurement campaigns.

In the following, a metaheuristic algorithm is used to optimize the clutter losses of several regions within a target radio network. This is done over groups of network cells within different regions of the target network, e.g. agricultural, urban or hilly. In terms of coverage planning, a regional classification of signal losses due to clutter improves the accuracy of the radio-coverage prediction.

In contrast to the parameter tuning of the mathematical model presented in Section 1.3, an analytical approach is not used for tackling this problem. Instead, the DASA metaheuristic algorithm (see Chapter ???, Section ???) is the tool of choice for optimizing the signal losses due to clutter.

There are several reasons for choosing the DASA as the optimization algorithm in the context of this problem. First, the benefits of metaheuristic algorithms for solving optimization problems, particularly in the context of radio networks, has been demonstrated by several authors **????** in general, and in this thesis in particular (see Chapter ??? and ???). Second, in **?**, the authors validated the suitability of the algorithm for solving numerical problems.

1.4.1 Optimization objective

The optimization objective consists of adjusting the loss values of the different clutter categories, i.e., $pl_{\text{CLUT}}(d_{(x,y)})$ from Equation (???) in Section ???, according to a set of field measurements of multiple cells covering a given geographical region. The same three data sets used in Section 1.3.3 are used in for the clutter-optimization problem: the first for Net_8, the second for Net_9, and the third for Net_{10}. Each region is independently optimized, so that the radio-propagation predictions of each set of network cells minimizes the mean-squared error against the field measurements, i.e.,

$$\min f_{\text{clut}} \quad = \quad \sum_{i=1}^{m_c} \frac{(p_c - pl_c(i, \beta_c^*) - fm_i)^2}{m_C} \quad \forall c \quad \in \quad C, \quad (1.2)$$

where f_{clut} is the optimization objective to be minimized in each of the three regions, p_c is the transmit power of cell c, fm_i is the i-th field measurement of cell c, the set of which has cardinality m_c, and m_C is the number of field measurements of all the cells within a given region. Similar to the least-squares approach in Section 1.3.2, $pl_c(i, \beta_c^*)$ represents the path loss of cell c at the same geographical point of the i-th field measurement, and β_c^* denotes the fitted parameter values of the prediction model for cell c.

For a reference of the different clutter categories used by the radio-propagation model, see Table 1.1.

1.4.2 Differential ant-stigmergy algorithm

As it has been mentioned before, the optimization algorithm we have chosen for the clutter-optimization problem is the DASA (see Chapter ???, Section ???). The mapping between the clutter-optimization problem and DASA is as follows

$$X_a = \{x_0, x_1, \ldots, x_i, \ldots, x_{11}\} \quad (1.3)$$

where X_a is the solution vector of ant a during the minimization process, and x_i represents the i-th clutter category within a given region or network. At the end of every iteration, and after all the ants have created solutions, they are evaluated to establish if any of them is better than the best solution found so far.

1.4.3 Simulations

In this case, one simulation round consists of multiple iterations of several steps. An iteration begins by generating a solution vector for each of the ants in the DASA colony. The following

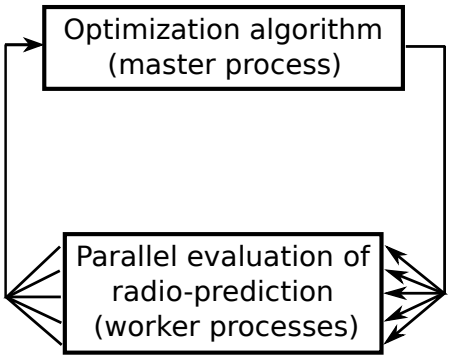

Figure 1.6: PRATO architecture and data flow during the clutter-optimization phase. The optimization algorithm runs on the master process, while the radio-propagation predictions of the involved network cells run in parallel over several worker processes.

step involves the parallel evaluation of the solution vector carried by an ant, i.e., one radio-propagation prediction per worker process. The final step is calculating the objective-function value, as defined in Equation (1.2), before sending it back to the master process for the DASA to generate the next set of solutions. Figure 1.6 depicts the way PRATO performs the parallel objective-function evaluation over the worker processes, while the optimization algorithm runs on the master process.

As opposed to the least-squares case, presented in Section 1.3.3, a much larger number of evaluations is needed for this kind of optimization. Therefore, it is essential to exploit the parallel nature of the framework in order to simultaneously evaluate the radio-coverage prediction of multiple cells. Otherwise, a metaheuristic approach would not be feasible, due to the computational time required to reach a reasonable solution.

The default clutter-loss values (in dB) for each clutter category, which are listed in the second column of Table 1.4, were provided by the radio experts of the Radio Network department at Telekom Slovenije, d.d. These values were empirically calculated using a classical (i.e., manual) approach, the results of which are regularly loaded into a commercial radio-planning application in order to validate the radio coverage at a network-wide level. The radio experts also suggested limiting the optimized clutter-loss values to a maximum of 40 dB.

The stopping criteria for the optimization runs involves limiting the maximum number of objective-function evaluations. In this sense, the limits for Net_8 and Net_{10} were set the 200, whereas for Net_9 the value was 500, since this network contains the largest number of cells. Overall, the framework completed 48,000 objective-function evaluations, i.e., 576,000 radio-coverage predictions for Net_8 and 288,000 for Net_{10}, whereas for Net_9 the number of objective-function evaluations was 120,000, for a total of 15,600,000 radio-coverage predictions.

Regarding the parameters that control the behavior of the DASA, they were set to the following values

- $m = 240$, the number of ants;
- $b = 10$, the discrete base;
- $q = 0.2$, the pheromone dispersion factor;
- $s_+ = 0.01$, the global scale-increasing factor;
- $s_- = 0.01$, the global scale-decreasing factor; and

Table 1.4: Clutter-category losses after the optimization. The default losses for each clutter category are given along the solutions for each of the test networks. All values are expressed in dB.

Clutter category	Default	Net_8	Net_9	Net_{10}
0	5.0	13.71	11.30	17.90
1	15.0	12.39	16.67	-
2	13.0	16.04	17.04	15.69
3	28.0	19.59	18.01	23.00
4	12.0	11.48	9.71	10.80
5	20.0	16.26	11.62	16.26
6	15.0	-	-	-
7	8.0	-	13.49	-
8	5.0	-	13.50	-
9	1.0	17.50	5.60	-
10	20.0	8.26	16.75	16.63
11	8.0	-	18.93	-

- $e = 1.0^{-2}$, the maximum parameter precision.

1.4.4 Results

The results achieved by the optimization process are shown in Table 1.4. The solutions are given for each of the test networks, along with the empirically-calculated (default) loss values due to clutter. Hyphens represent clutter categories for which there are no field measurements available. Consequently, it is not possible to evaluate the objective-function for them.

The optimized loss for the first clutter category, 0, representing urban area without buildings, is larger than the default value in all three networks. This may be attributed to the fact that these areas are not completely open, mostly surrounded by forests (Net_8 and Net_{10}) and buildings of different sizes (Net_9). As for the category 1, representing suburban area, the value for Net_8 is lower than the default one, mainly because this network is deployed over a predominant agricultural area, i.e., suburban areas are less dense here. On the other hand, the value for Net_9 is larger, indicating a building density above the average, whereas for Net_{10}, the value could not be calculated due to lack of measurements. For the category 2, representing urban area, the optimized values are above the default ones, clearly showing an underestimation of the manual approach. However, the relation among the clutter losses corresponds with the population density in each of the regions, being Net_{10} the less dense urban area among the three networks. The optimized values of the category 3, representing dense urban area, are lower than the default ones. This indicates that the dense urban areas in these regions have a lower density than the average case. Representing agricultural area, the category 4 gets a value very close to the default one for Net_8 and Net_{10}, whereas for Net_9 the value is lower, indicating that this type of land is mostly open near the city, e.g., without plantations. As for the category 5, representing forests, the results correspond with the type of forest that dominates each of the test-network regions. Namely, Net_8 and Net_{10} are dominated by dense forests presenting leave foliage, whereas in Net_9 the forests are mostly coniferous and more sparse. Keeping the most of the default loss values for the categories 6, 7 and 8, the results of the next category, 9, representing water, indicate creeks and rivers in these area are almost entirely surrounded by forests (Net_8) or buildings (Net_9), since none of the regions lays by the sea. As for the industrial area, denoted by the clutter category 10, lower loss values than the empirically-calculated defaults appear. This indicates

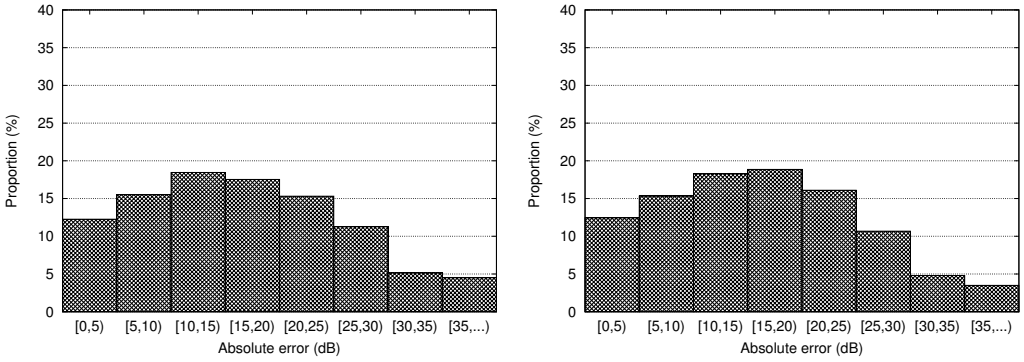

Figure 1.7: Error distribution of the radio prediction for network Net_8: (a) with fitted parameter values and default clutter losses, and (b) with fitted parameter values and optimized clutter losses.

the presence of sparse industrial buildings in Net_8, and a higher density of mostly commercial buildings for Net_9 and Net_{10}. The last clutter category, 11, could not be calculated for Net_8 and Net_{10} due to lack of field measurements.

Notice that the relationships among the different clutter categories is correctly kept for the three test networks. For example, it can be observed that the clutter loss for dense urban area (category 3) is higher than the values of the urban area (category 2), as well as of the agricultural area (category 4). Hence, the results reflect physically feasible losses, despite the higher deviation from the default losses shown by the category 2, and the lower deviation for the category 3, again with respect to the default losses. Such relations hold for different categories of all three test networks, strongly suggesting the correctness of the applied optimization approach and the evaluation methodology used. Consequently, it can be confirmed that the combination of PRATO and a metaheuristic algorithm is applicable for performing optimization of clutter losses, since it is capable of reflecting the physical phenomena appearing in real-world conditions and improving the quality of radio-propagation predictions for three, geographically different radio-network instances.

Similar to Section 1.3.4, bar charts show the cumulative distribution of the absolute error between the signal-propagation prediction and the field measurements (see Figures 1.7, 1.8, and 1.9). Figure 1.7 (a) depicts the error distribution of the prediction for test network Net_8 using the fitted model parameters, whereas Figure 1.7 (b) shows the absolute-error distribution for the same test network, but using the optimized clutter losses (see Table 1.4, column Net_8). Notice how the error distributions show an improvement when the optimized clutter losses are used, lowering the biggest (right-most) deviations even more.

The error distributions of the radio-propagation predictions for test network Net_9 using fitted parameters and default clutter losses, and fitted parameters with optimized clutter losses are shown in Figures 1.8 (a) and 1.8 (b), respectively. Similar to Net_8, the improvement appears in the biggest deviations, since their values are lower than when using the default clutter losses.

For the last test network, Net_{10}, the error distributions are depicted in Figure 1.9 (a) using the default clutter losses, and Figure 1.9 (b) for the optimized ones. Again, fitted model parameters are used for both simulation sets. In this case, a more significant improvement than for the other two networks appears, clearly showing the favorable effect of the optimization process. Moreover,

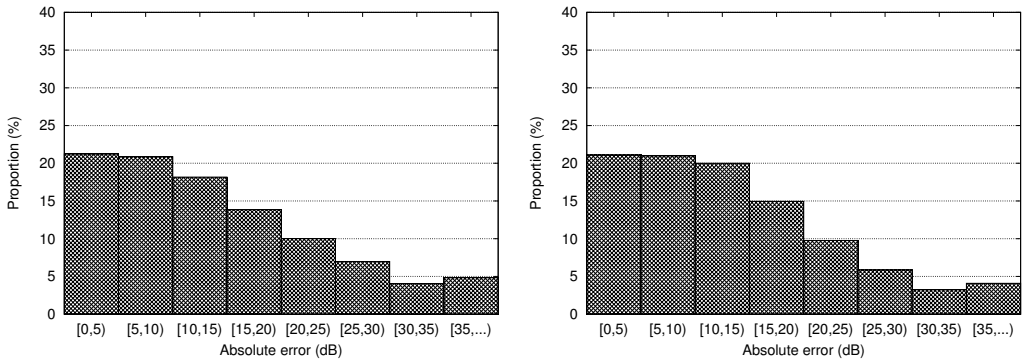

Figure 1.8: Error distribution of the radio prediction for network Net_9: (a) with fitted parameter values and default clutter losses, and (b) with fitted parameter values and optimized clutter losses.

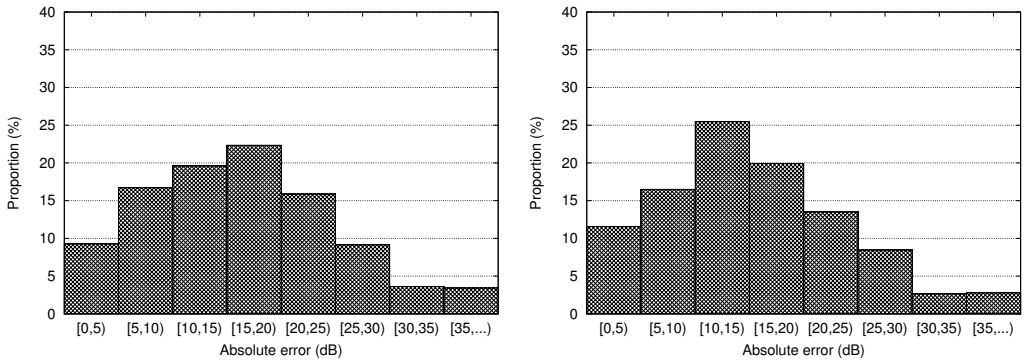

Figure 1.9: Error distribution of the radio prediction for network Net_{10}: (a) with fitted parameter values and default clutter losses, and (b) with fitted parameter values and optimized clutter losses.

Table 1.5: Statistical analysis of the optimization solutions for each test network. All values are expressed in dB. The corresponding box plots are depicted in Figure 1.10.

	Net_8				Net_9				Net_{10}			
Cat.	Min	Max	Avg	St.dev.	Min	Max	Avg	St.dev.	Min	Max	Avg	St.dev.
0	13.36	13.97	13.71	0.15	11.22	11.40	11.30	0.04	17.72	17.85	17.90	0.07
1	-	-	-	-	14.25	19.20	16.67	1.87	-	-	-	-
2	15.84	16.21	16.04	0.08	16.99	17.11	17.04	0.03	15.64	15.72	15.69	0.03
3	19.15	20.07	19.59	0.25	17.95	18.12	18.01	0.04	22.68	23.20	23.00	0.16
4	11.35	11.62	11.48	0.05	9.63	9.77	9.71	0.03	10.73	10.84	10.80	0.03
5	16.00	16.54	16.26	0.14	11.45	11.80	11.62	0.08	16.19	16.30	16.26	0.04
6	-	-	-	-	-	-	-	-	-	-	-	-
7	-	-	-	-	12.71	14.52	13.49	0.39	-	-	-	-
8	-	-	-	-	12.25	15.79	13.50	0.83	-	-	-	-
9	16.07	18.80	17.50	0.83	4.67	6.26	5.60	0.35	-	-	-	-
10	7.79	8.54	8.26	0.19	16.68	16.87	16.75	0.05	16.50	16.68	16.63	0.07
11	-	-	-	-	18.62	19.20	17.04	0.13	-	-	-	-

this result suggests that some of the default clutter losses considerably fail in representing the actual physical conditions in the geographical region of this network.

The presented results confirm that the optimization of clutter losses with respect to field measurements improves the quality of the calculated radio-propagation predictions. Considering the default clutter losses were empirically calculated by the radio engineers for the whole network, the convenience of the automated optimization procedure is clear. Indeed, these advantages are a consequence of a simpler method that automatically delivers radio-predictions of superior quality, thus accurately representing the physical properties of a given environment.

Because of the stochastic nature of the optimization algorithm, the results of 30 independent runs were collected in order to have enough data for them to be statistically relevant. In other words, the robustness of the solutions, that have been presented in the previous section, is analyzed here.

To this end, Table 1.5 shows the solutions reached by the DASA for each of three test networks. The calculated signal losses are depicted with the minimum, maximum and average values for every clutter category, along with their standard deviations. Again, hyphens represent clutter categories for which there are no field measurements available, and thus they could not be optimized. In order to easily visualize the data shown in Table 1.5, box plots based on the same values are provided in Figure 1.10. It can be observed that the standard deviation is low for almost all optimized categories, indicating a consistent convergence of the optimization algorithm. However, some exceptions are noticeable, e.g., the category 9 in Net_8 and Net_9, representing water. In this case, there is a lower density of field measurements nearby water trails since none of the test networks lays by the sea. Regarding the categories 1 (suburban area), 7 and 8 (dry open land area) of Net_9, we again find very few field measurements over this areas, thus higher standard-deviation values appear. Based on these findings, the standard deviation of the optimized clutter losses can be considered a quantity indicator of the field measurements required by the optimization process, i.e., a higher standard deviation denotes more field measurements are needed to optimize the target clutter category.

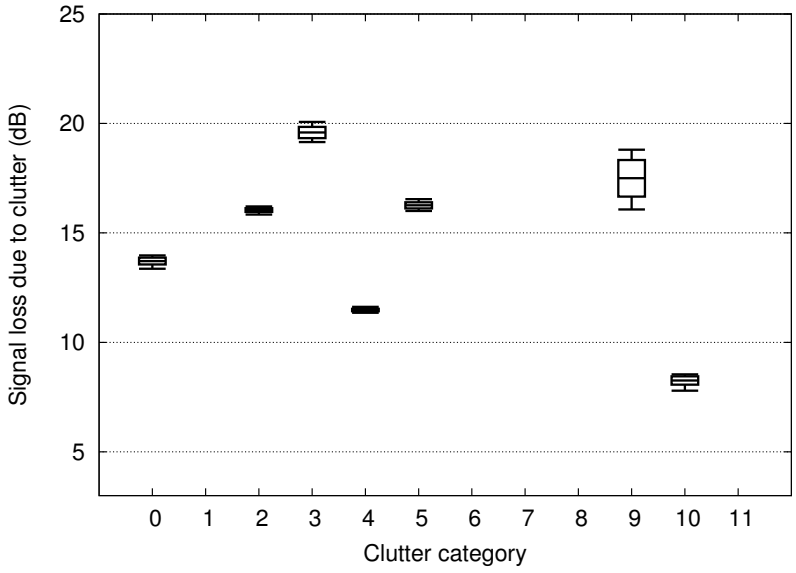
Signal loss due to clutter (dB)
25
20
15
10
5
0 1 2 3 4 5 6 7 8 9 10 11
Clutter category

(a)

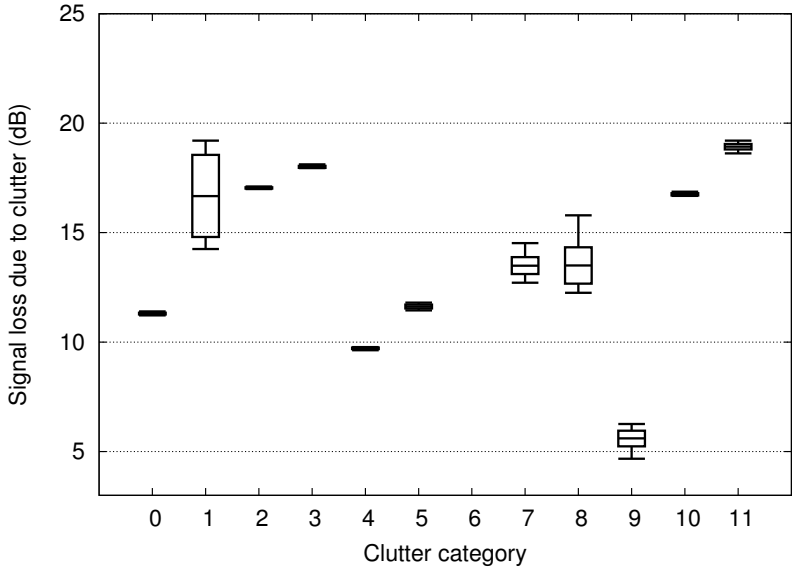
Signal loss due to clutter (dB)
25
20
15
10
5
0 1 2 3 4 5 6 7 8 9 10 11
Clutter category

(b)

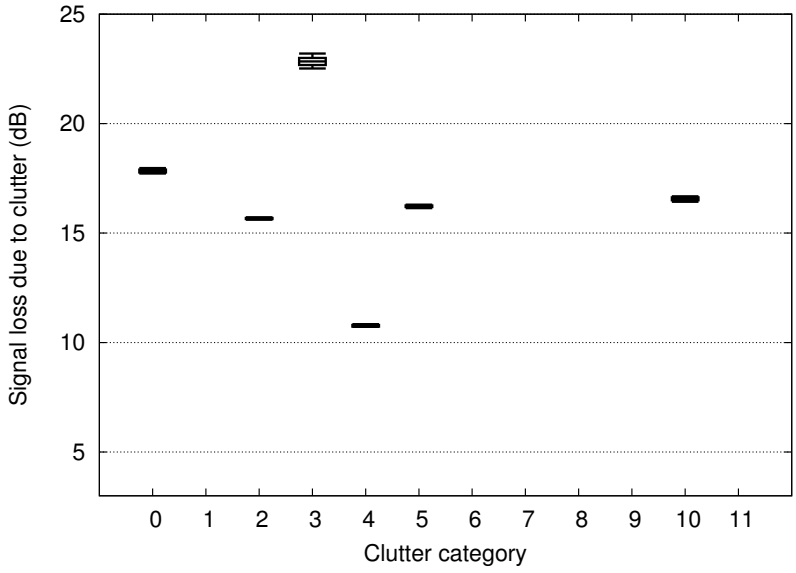

(c)

Figure 1.10: Box plots representing the statistical-analysis values of Table 1.5, for the solutions of the clutter-optimization process of each test network: (a) Net_1, (b) Net_2, and (c) Net_3.

1.5 Summary

This chapter shown the suitability of PRATO as a network-planning tool by tackling two coverage-planning problems, which were tested over the newly deployed LTE network in Slovenia. The first one involved the parameter tuning of the empirical radio-propagation model using a snapshot of field measurements. The second one considered the optimization of the clutter losses over different regions of the country, therefore adapting them to the local conditions of the geographical region of each network.

The combination of the afore-mentioned techniques with PRATO provides an environment-adaptable framework for radio-network planning. This delivers a tool with a considerable improvent of the solution accuracy of the analyzed instances, especially if compared to traditional, i.e., manual or semi-automated, coverage-planning methods.

Additionally, the simulation results indicate that PRATO is applicable for planning and optimization of real-world radio networks, since it is capable of tackling bigger problem instances in a feasible amount of time. Particularly, several of the presented instances show a large computational-time complexity, which is beyond reach for a serial implementation of an automated approach. Moreover, the parallelization capabilities provided by the framework create new problem-solving possibilities. Indeed, even computational-intensive tasks such as stochastic optimization, which involves millions of radio-prediction evaluations, are feasible if PRATO is used.